Extracellular vesicles from tonsil-derived mesenchymal stromal cells show anti-tumor effect via miR-199a-3p

DA-WON CHOI[1,2*], KYUNG-AH CHO[1*], JUNGWOO KIM[1], HYUN-JI LEE[1], YU-HEE KIM[1], JANG-WON PARK[3] and SO-YOUN WOO[1]

[1]Department of Microbiology, College of Medicine, Ewha Womans University; [2]System Biohealth Brain Korea 21, Ewha Womans University; [3]Department of Orthopaedic Surgery, College of Medicine, Ewha Womans University, Seoul 07804, Republic of Korea

Received July 27, 2021; Accepted October 5, 2021

DOI: 10.3892/ijmm.2021.5054

Abstract. Mesenchymal stem cells (MSCs) are mesoderm-originated adult SCs that possess multidirectional differentiation potential. MSCs migrate to injured tissue and secrete a range of paracrine factors that induce regeneration in damaged tissue and exert immune modulation. Because tumor progression is dependent on cross-talk between the tumor and its microenvironment, MSCs also produce extracellular vesicles (EVs) that mediate information transfer in the tumor microenvironment. However, the effect of MSC-derived EVs on tumor development and progression is still controversial. To date, tonsil-derived MSCs (T-MSCs) have been shown to possess all the defined characteristics of MSCs and show distinctive features of differential potential and immune modulation. To observe the effect of soluble mediators from T-MSCs on tumor growth, human liver cancer cell line (HepG2) cells were injected into nude mice and HepG2 cell scratch migration assay was performed using conditioned medium (CM) of T-MSCs. T-MSC CM inhibited tumor growth and progression and it was hypothesized that EVs from T-MSCs could inhibit tumor progression. microRNA (miRNA or miR) sequencing using five different origins of T-MSC-derived EVs was performed and highly expressed miRNAs, such as miR-199a-3p, miR-214-3p, miR-199a-5p and miR-199b-5p, were selected. T-MSCs inhibited tumor growth and HepG2 cell migration, potentially via miR-199a-3p targeting CD151, integrin α3 and 6 in HepG2 cells.

Correspondence to: Professor So-Youn Woo, Department of Microbiology, College of Medicine, Ewha Womans University, 25 Magokdong-ro 2-gil, Gangseo, Seoul 07804, Republic of Korea
E-mail: soyounwoo@ewha.ac.kr

*Contributed equally

Key words: tonsil-derived mesenchymal stromal cells, microRNA, exosome, tumor suppression

Introduction

Mesenchymal stem cells (MSCs) are mesoderm-derived adult SCs that possess multidirectional differentiation potential (1). Although bone marrow (BM) is the primary site for MSC isolation, MSCs are also located in the perivascular space of various types of tissue expressing CD146, including dental pulp, adipose tissue, neonatal placenta, amniotic membrane and umbilical cord (2). Our previous study isolated tonsil-derived MSCs (T-MSCs) (3) and showed their various lineage differentiation potentials and immune modulatory effects (4). Compared with MSCs of other origins, T-MSCs possess distinctive features, such as CD106 (vascular cell adhesion protein 1), CD166 (5) and CD274 [programmed death ligand-1 (PD-L1)] (6) expression.

MSCs migrate to injured tissue and secrete a range of paracrine factors that induce regeneration in damaged tissue. MSCs contribute to tissue repair primarily via paracrine factors and stimulation of target cells, but not by replacement of injured tissue (7). MSCs mediate fibrosis [keratinocyte growth factor, hepatocyte growth factor (HGF), vascular endothelial (VE GF, Angiopoietin-1, stromal cell-derived factor-1, insulin-like (I GF-1, epidermal (E)GF, nerve GF and transforming (T)GF-α], angiogenesis [angiogenin, VEGF, tissue inhibitor of metalloproteinases 1 (TIMP-1), TIMP-2 and matrix metalloproteinase (MMP)-1], immune modulation (IL-10, IL-13, IFN-γ, IL-12, prostaglandin E2, indoleamine 2,3-dioxygenase, heme oxygenase-1 and galectins), chemotaxis [C-C motif chemokine ligand (CCL)5, C-X-C motif chemokine ligand (CXCL)12 and CCL8], apoptosis [HGF, IGF-1, osteopontin, growth hormone) and proliferation (EGF, TGF-α, HGF, bFGF, IGF binding protein and macrophage colony-stimulating factor) through various factors (8). Consequently, culture medium conditioned by MSCs produces therapeutic effects similar to those observed in cell delivery studies using mouse models of acute myocardial infarction (9) and lung injury (10). The active fraction of conditioned medium (CM) contains particles released from the cells, collectively called extracellular vesicles (EVs) (11). Cells produce EVs, including both microvesicles (>200 nm) and exosomes (50-200 nm), via intracellular vesicle sorting processes. EVs do not contain functional nuclei and are

only surrounded by lipid bilayer. EV are secreted by endothelial, immune and smooth muscle cells and platelets (11). Common MSC EV markers include CD9, CD63, CD81, tumor susceptibility gene 101 (TSG101) protein and heat shock protein 70 (12,13). MSC-derived EVs act on target cells by transferring mRNAs, microRNAs (miRNAs or miRs), lipids and proteins, which alter the activity of target cells (14).

Cross-talk between the tumor and tumor microenvironment may be key for tumor growth and development (15). MSCs may contribute to tumor development by migrating to inflammatory or cancer sites and evolve into tumor-associated MSCs and fibroblasts, thereby activating cell proliferation, invasion, angiogenesis and metastasis (16). This interaction between tumor cells and MSCs is primarily mediated by EVs (17). MSCs also produce EVs that mediate information transfer in the tumor microenvironment; for example, BM-MSC-derived exosomes induce apoptosis and cell cycle arrest in HepG2 cells (18). Although the effect of MSC-derived EVs on tumor development and progression is still unknown, the use of MSC-derived EVs as cancer modulators is preferable to using the cellular form of MSCs due to the small size and homogeneity of EVs (19). The present study aimed to identify the potential effect of T-MSC-derived EVs on tumor development using the human liver cancer cell line HepG2.

Materials and methods

Cell culture and CM collection. HepG2 cells were purchased from American Type Culture Collection and additional STR profiling was performed (Fig. S1). T-MSCs previously obtained from patients (Ewha University Medical Center Institutional Review Board; approval no. EUMC 2018-01-011-002) at Ewha Womans University Seoul Hospital (Seoul, Korea) were maintained as previously described (20). Patients provided informed written consent for the use of their tissue.

Phenotype analysis. To analyze cell phenotype, T-MSCs were washed with FACS buffer (0.5 FBS and 0.1% NaN_3 in PBS), blocked with 0.5 μg/ml purified rat anti-mouse CD16/CD32 (BD Pharmingen) at 4˚C for 5 min and stained with FITC anti-CD11b (cat. no. ICRF44, mouse IgG_1, κ), FITC anti-CD45 (2D1, mouse IgG_1, κ), FITC anti-CD73 (AD2, mouse IgG_1, κ), FITC anti-CD90 (5E10, mouse IgG_1, κ), FITC anti-CD105 (43A3, mouse IgG_1, κ) and FITC mouse IgG_1, κ isotype (MOPC-21) antibodies (all BioLegend, Inc.) at 0.5 μg/ml for 20 min at room temperature. After staining, the cells were fixed with 4% paraformaldehyde (PFA, Sigma-Aldrich; Merck KGaA) in phosphate-buffered saline (PBS) to final 0.5% PFA. Stained cells were acquired using a Novocyte flow cytometer (ACEA Bioscience, Inc.). Acquired cells were analyzed by FlowJo software (v10, TreeStar, Inc.).

Adipogenic differentiation. For adipogenic differentiation, T-MSCs were seeded at a density of $1x10^4$ cells/well in a 12-well plate and cultured with adipogenic medium (Invitrogen; Thermo Fisher Scientific, Inc.) in a humid atmosphere with 5% CO_2 at 37˚C for 3 weeks. Medium was replaced every 3-4 days. After 3 weeks, adipogenic cultures of T-MSCs were rinsed with PBS and fixed in 4% PFA for 5 min at room temperature. The wells were dried completely and stained with Oil red O (Sigma-Aldrich; Merck KGaA) for 10 min at room temperature. The Oil red O solution was removed and wells were immediately washed with distilled water four times. Wharton's jelly-derived (WJ-)MSCs were purchased from PromoCell GmbH. Ethics approval was received for the use of primary cells (Ewha Institutional Biosafety Committee; approval no. IBC-past-096). HepG2 cells were cultured in Minimum Essential Medium Eagle (MEM; Welgene, Inc.) with 10 FBS (Welgene, Inc.) and 1% penicillin/streptomycin solution (P/S; Capricorn Scientific GmbH) in a humid atmosphere with 5% CO_2 at 37˚C. T-MSCs and WJ-MSCs were cultured in low-glucose Dulbecco's modified Eagle medium (DMEM; Welgene, Inc.) with 10 FBS (Welgene, Inc.) and 1% P/S in 100-mm cell culture plates. For preparation of T-MSC CM (T-CM), T-MSCs at 80% confluence were washed four times with PBS (Welgene, Inc.) and medium was replaced with serum-free DMEM. The medium was collected after 48 h, centrifuged at 190 x g for 5 min at room temperature, passed through a 0.2-μm filter (MilliporeSigma) and concentrated 20-fold using a 3-kDa Amicon Ultra centrifugal filter unit (EMD Millipore) with high-speed centrifugation (Sorvall LYNX4000; Thermo Fisher Scientific, Inc.) at 5,000 x g for 1 h at 4˚C. T-CM for animal experiments was frozen, whereas T-CM and CM from WJ-MSCs for exosome isolation and reverse transcription-quantitative (RT-q)PCR were used immediately.

Isolation of T-MSC EVs. For EV isolation, Minimal Information for Studies of EVs (MISEV) 2018 guidelines proposed by the International Society for EVs (ISEV) were referred to for separation and characterization (11).

To isolate EVs from T-MSCs, 1/5 volume of ExoQuick-TC reagent (System Biosciences) was added to 10 ml T-CM and mixed by vigorous inverting. Following incubation at 4˚C overnight, the mixture was centrifuged at 1,500 x g for 30 min at 4˚C. The supernatant was removed, and final centrifugation at 1,500 x g was performed for 5 min at room temperature. The visible EV-containing pellet was resuspended in 100-500 μl PBS for Nanosight particle tracking analysis (Nanosight NS300; Malvern Instruments, Ltd.) and for protein concentration analysis via bicinchoninic acid (BCA) protein assay (Thermo Fisher Scientific, Inc.). Following BCA assay, 6X SDS-PAGE loading buffer was added for sample preparation for immunoblotting and stored at -80˚C until use.

Transmission electron microscopy (TEM). Purified EVs were diluted to 1:1,000 in PBS. A total of 5 μl diluted EVs was dropped on Formvar-carbon-coated EM grids. The grids were stained with 2% uranyl acetate for 2 min at room temperature and removed using filter paper. Finally, the grids were viewed using a H-7650 TEM (Hitachi, Ltd.) at 80 kV. Digital images were captured at a magnification of 70,000-200,000.

Scanning EM (SEM). Diluted EVs were dropped on Poly L-lysine cover glass and prefixed with 0.25% glutaraldehyde for 30 min at room temperature. After washing in PBS, samples were maintained in 1% osmium tetroxide for 30 min

for final fixation at room temperature. Then, samples were washed and dehydrated by serial dilution with ethanol and critical point drying. Finally, samples were mounted onto stubs, sputter-coated with gold by Quorum Technologies and examined with a Sigma-300 microscope (Zeiss GmbH) at a magnification of x70,000.

Animal experiments. Male BALB/c nude mice (n=6, age, 5 weeks; weight, 18±2 g) were purchased from OrientBio. All animals were housed at 21-23˚C and 51-54% humidity in a pathogen-free environment on a 12/12-h light/dark cycle and allowed free access to food and water. All animals were monitored every day for health and behavior. The method of euthanasia was carbon dioxide inhalation followed by cervical dislocation (20% vol/min for a cage size of 8x13x5 inches) and animal death was confirmed by cardiac and respiratory arrest. The experimental procedures were approved by the Animal Care and Use Committee of the College of Medicine, Ewha Womans University (Seoul, Korea; approval no. EUM18-0408). To construct a hepatoma xenograft model, $3x10^6$ HepG2 cells were suspended in 100 μl low-glucose DMEM and injected subcutaneously into the right back of each animal (n=3) (21). To assess the effect of T-CM, HepG2 cells were suspended in 100 μl CM from $5x10^5$ T-MSCs and injected at the same position (n=3). Five days after the injection, mice were euthanized by carbon dioxide and cervical dislocation and the tumor was isolated, chopped and seeded onto a 100-mm cell culture plate. Images were captured following 2 and 9 days of culturing in a humid atmosphere with 5% CO_2 at 37˚C using an inverted light microscope (Olympus Corporation) at x100 magnification, and cell clusters were calculated manually by counting cluster of >50 cells.

Immunoblotting. Equal concentrations of EV (5 μg/lane) from T-MSCs were loaded onto 5% stacking/10% separating sodium dodecyl sulfate (SDS)-PAGE, separated by electrophoresis, transferred to polyvinylidene difluoride (PVDF) membranes, blocked with 5% skimmed milk in TBST (50 mM Tris HCl, pH 7.6, 150 mM NaCl, 0.1% Tween-20) for 1 h at room temperature and incubated with primary antibodies overnight at 4˚C. Gels were stained with Coomassie blue solution (0.1 Coomassie brilliant blue R-250, 40.0 methanol and 10.0% acetic acid in water) overnight at room temperature followed by incubation with de-staining solution (40 methanol and 10% acetic acid in water) for 2 h at room temperature. All primary antibodies were prepared by diluting in 3.00 BSA (Bovogen Biologicals Pty, Ltd.) and 0.02% sodium azide (Sigma-Aldrich; Merck KGaA) in TBST. Anti-CD63 mouse monoclonal antibody (cat. no. ab193349; 1:1,000; $IgG_1\kappa$) was purchased from Abcam; anti-CD81 (cat. no. sc-166029; 1:200; $IgG_{2b}\kappa$) and anti-β-actin mouse monoclonal antibody (cat. no. sc-47778; 1:3,000; $IgG_1\kappa$) were purchased from Santa Cruz Biotechnology, Inc. PVDF membranes were washed three times for 10 min each in TBST and incubated with horseradish peroxidase-conjugated goat anti-mouse IgG (H+L) antibody (cat. no. #1706516; BioRad Laboratories, Inc.), diluted in TBST (1:4,000), for 1 h at room temperature. Following incubation, the membranes were washed three times for 10 min each in TBST and developed using an EZ-Western Lumi Femto Western blot kit (Doo Gene Bio Co., Ltd.). Images were obtained using ImageQuant LAS 3000 (FUJIFILM Wako Pure Chemical Corporation). The pixel densities of protein bands were analyzed using UN-SCAN-IT-gel 6.1 software (Silk Scientific, Inc.).

Cell transfection. METAFECTENE PRO (Biontex Laboratories GmbH) was used according to manufacturer's protocol to transfect cells. Briefly, mixed solutions containing 1 μg AccuTarget™ fluorescein-labeled miRNA negative control, inhibitor #1 (cat. no. SMC-4101, Bioneer, bioneer.co.kr/20-smc-4101.html) or has-miR-199a-3p inhibitor (Bioneer) were added to 50 μl serum-free medium. Then, 3 μl METAFECTENE PRO was added to 50 μl serum-free medium at room temperature for 20 min. The sequence of has-miR-199a-3p inhibitor was 5'-ACAGUAGUCUGC ACAUUGGUUA-3.' Following incubation, the mixture was carefully added to cells. After 5 h, cells were collected for RT-qPCR and wound healing assay was performed.

miRNA sequencing and target gene prediction. CM from five different donor originated T-MSCs and DMEM (negative control) were sent to Macrogen, Inc. for miRNA sequencing by SMARTer smRNA-Seq method (22) using TruSeq Small RNA Library Prep kit (RS-200-0012, Illumina, Inc.).Ribosomal RNA removed reads were aligned to reference genome (miRBase v22.1) and non-coding RNA database (RNAcentral 14.0) to classify known miRNA and other type of RNA. Novel miRNA prediction is performed by miRDeep2 (v2.0.0.8). To reduce systemic bias, size factors from the count data were estimated and Trimmed Mean of M-values normalization with edgeR R library was applied. Statistical analysis was performed using Fold Change, exact-Test using edgeR per comparison pair. Hierarchical clustering analysis was also performed using complete linkage and Euclidean distance as a measure of similarity to display the expression patterns of differentially expressed miRNAs that satisfied the |fold-change|≥2 and $P<0.05$ criteria. All data analysis and visualization of differentially expressed genes was performed using R 3.3.1 (r-project.org). miRNA target gene prediction was performed by TargetScanHuman 7.2 (targetscan.org/vert_72/). In order to analyze signaling pathways associated with miRNA from exosomes, miRNA-target genes were analyzed by Kyoto Encylcopedia of Genes and Genomes (KEGG) analysis. Genes derived from mirDIP were further analyzed by Database for Annotation, Visualization and Integrated Discovery v6.8 to identify enriched biological pathways.

RT-qPCR. To isolate miRNA, T-CM and CM from WJ-MSCs was added to an appropriate volume of Exo2D™ for RNA (ExosomePlus) according to the manufacturer's protocol, and inverted several times. The mixture was incubated at 4˚C for 30 min and centrifuged at 3,000 x g for 30 min at 4˚C. The supernatant was removed and resuspended in 100 μl PBS and the RNA concentration was measured by BioPhotometer D30 (Eppendorf) and adjusted to 1 μg/μl. miRNA was converted into complementary DNA (cDNA) using MystiCq™ microRNA cDNA Synthesis Mix (Sigma-Aldrich; Merck KGaA) according to the manufacturer's protocol. MystiCq Universal PCR Primer (Sigma-Aldrich; Merck KGaA) was used as a reverse primer

for RT-qPCR. MystiCq microRNA qPCR Control Primer RNU6-1 (cat. no. MIRCP00001) and MystiCq microRNA qPCR Assay Primer hsa-miR-199a-3p (cat. no. MIRAP00244; both Sigma-Aldrich; Merck KGaA) were used as forward primers. Total RNA was extracted using an RNeasy Plus Mini kit (Qiagen GmbH) to isolate RNA of transfected HepG2 cells. Total RNA (1 μg) was transcribed into cDNA using RT reagent (ElpisBiotech, Inc.), and RT-qPCR was performed. Primer sequences were as follows: CD151 forward, 5'-ATGGGTGAG TTCAACGAGAAGA-3' and reverse, 5'-GCAGGCTGATGT AGTCACTCT-3'; integrin α3 (ITGA3) forward, 5'-TGTGGC TTGGAGTGACTGTG-3' and reverse, 5'-TCATTGCCTCGC ACGTAGC-3'; ITGA6 forward, 5'-ATGCACGCGGATCGA GTTT-3' and reverse, 5'-TTCCTGCTTCGTATTAACATG CT-3' and human GAPDH (192 bp) forward, 5'-GGTAAAGTG GATATTGTTGCCATCAATG-3'and reverse, 5'-GGAGGG ATCTCGCTCCTGGAAGATGGTG-3'. The mixture was prepared in each well of a Fast Optical 96-well reaction plate (Applied Biosystems; Thermo Fisher Scientific, Inc.) using 0.5 reverse/forward primer each, 10.0 1X SensiFAST SYBR Hi-ROX mix (Bioline; Meridian Bioscience, Inc.), 8.0 deionized water and 1.0 μl cDNA. Amplification was performed in triplicate with 40 cycles of 15 sec denaturation at 95˚C, 1 min annealing at 62˚C and 30 sec extension at 72˚C using StepOnePlus Real-Time RCR System (Applied Biosystems; Thermo Fischer Scientific, Inc.). The relative fold expression and changes were calculated using the $2^{-\Delta\Delta Cq}$ method (23).

Wound healing assay. A scratch wound healing assay was performed to compare the effect of T-CM or exosomes on the migration capability of HepG2. HepG2 cells ($2x10^5$) were seeded onto a 12-well cell culture plate with MEM containing 10% FBS and 1% P/S and incubated to 90-100% confluence at 37˚C in a 5% CO_2 incubator. When the confluence of cells was reached, a scratch wound was made in the cell monolayers using a cut cell scraper. The transfected cells were allowed to grow for an additional 24 and 48 h in the presence of CM or EVs (10 μg/ml) with serum-free MEM. Images were taken at 0, 24 and 48 h using an inverted light microscope (Olympus Corporation; x40 magnification). The migration distance was quantified using ImageJ software v1.53 g (imagej.nih.gov). The percentage of area closure was calculated as follows: Final wound width/initial wound width x100.

Statistical analysis. Data are presented as the mean ± SEM (n>3). Statistical significance was determined by one-way ANOVA with multiple comparison by Sidak test applied to the wound healing assay with T-CM or miRNA inhibitors. Paired t-test was used for wound area closure after T-CM treatment. Student t-test (unpaired) was used for the comparison of miR expression between WJ-MSCs and T-MSCs. All analyses were performed using Prism 9.2 (GraphPad Software, Inc.). $P<0.05$ was considered to indicate a statistically significant difference.

Results

T-CM suppresses tumor formation and migration of HepG2 cells. Investigation of the effect of subcutaneous injection of CM of T-MSCs at the right back of mice showed that T-CM with HepG2 cells formed a smaller tumor mass than injection of DMEM with HepG2 cells after 9 days (Fig. 1A). At 5 days after the injection, no mice had died and the plated cells from tumor masses were separated, chopped and seeded for culture. Formation of cell clusters was assessed at 2 and 9 days. The cell clusters in the HepG2 + T-CM group tumor mass were less prolific than those from the control group (Fig. 1B). Comparison of the number of clusters on culture plates (Fig. 1C) indicated that T-CM exerted an inhibitory effect on HepG2 cell tumor growth and expansion *in vitro*. The *in vitro* scratch assay compared the effect of T-CM on the migration of HepG2 cells were obtained after 24 and 48 h (Fig. 1D); the distance between the scratch of the control group (DMEM) was closer and the area became smaller as time passed. By contrast, in the T-CM group, wound area remained almost same as that at 0 h. These results suggested that T-CM had an inhibitory effect on the migration of HepG2 cells (Fig. 1E and F).

Isolation and characterization of T-MSC exosomes. The morphology of T-MSC small EVs isolated from CM and observed by TEM and SEM showed a round or oval shape with diameter <200 nm (Fig. 2A). Immunoblot analysis indicated positive expression of CD63 and CD81 (Fig. 2B). The particle size distribution and concentration of isolated exosomes were analyzed by Nanosight particle tracking analysis (Fig. S2). The mean diameter of particles was 192.3±21.6 nm and the concentration was $1.28x10^8$±$2.38x10^7$ particles/ml.

Exosomal miRNA hsa-miR-199a-3p suppresses migration of HepG2 cells. To search the highly expressed miRNAs in T-MSC EVs, five different origins of T-MSCs established in the lab were selected. These five T-MSCs showed typical surface markers of MSCs (Fig. S3A). For the comparison of differentiation potential, adipogenic differentiation of these five different T-MSCs was induced (Fig. S3B). After confirming these cells possessed chracteristics of MSCs [plastic adherence, phenotype marker expression ($CD73^+$, $CD90^+$, $CD105^+$, $CD45^-$ and $CD11b^-$) and adipocyte differentiation], miRNA sequening was performed. *Mycoplasma* contamination was not detected in small RNA composition report from Macrogen. The highly expressed miRNAs are listed in Table I. A heatmap (Fig. S4A) was constructed to demonstrate the results of hierarchical clustering analysis (Euclidean method, complete Linkage), which clusters the similarity of mature miRNAs and samples by expression level (normalized value) from a significant list. Fig. S4B shows the number of up- and downregulated mature miRNAs based on fold change compared with those of negative control. The upregulated miRNAs with similar expression levels were grouped together using the normalized value of each sample (Fig. S4C). Enriched signaling pathways among top 20 miRNA-target genes were analyzed by KEGG analysis; genes belonging to cancer pathway were highly enriched (Fig. S5). Exosomal RNA was extracted from T-MSC and WJ-MSC CM. To validate miRNA sequencing, hsa-miR-199a-3p, hsa-miR-214-3p, hsa-miR-199a-5p and hsa-miR-199b-5p expression levels were compared with expression of exosomal RNA from T-MSCs and WJ-MSCs by RT-qPCR. Expression

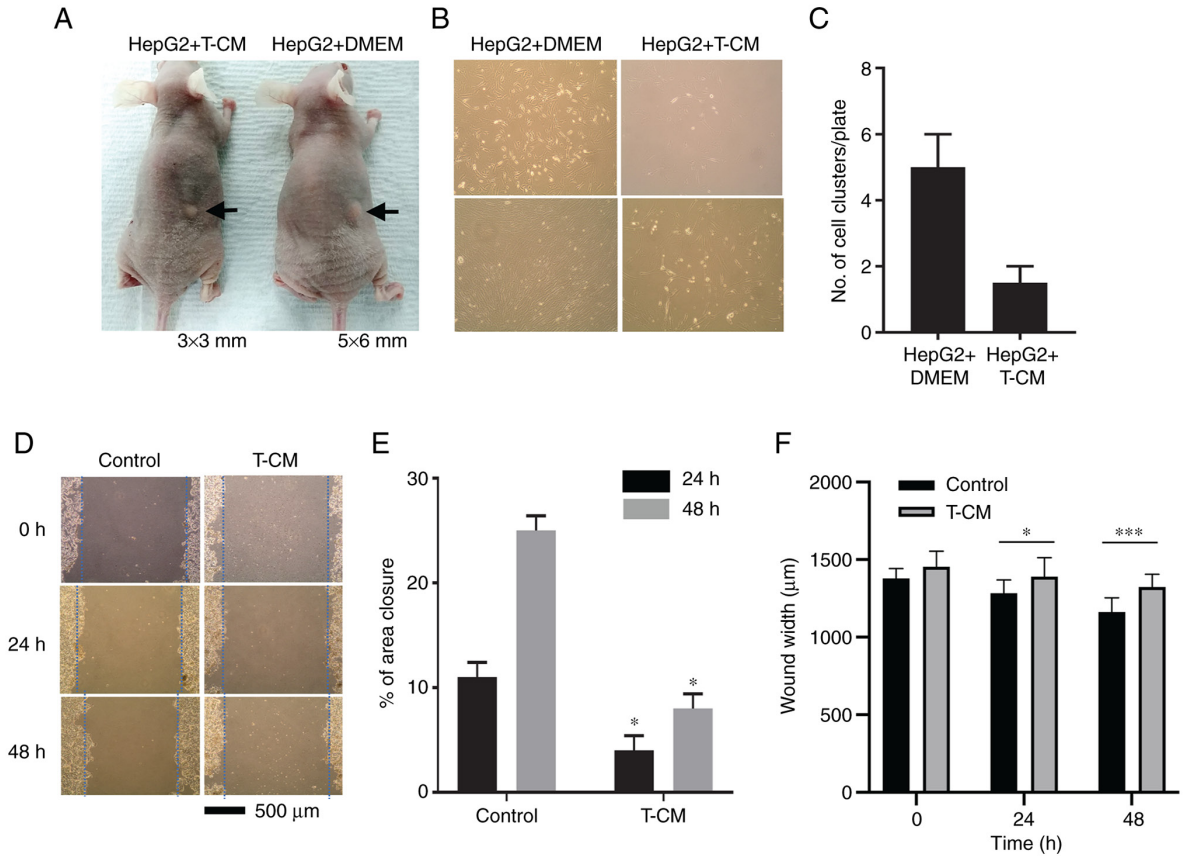

Figure 1. T-CM decreases tumorigenesis and migration of HepG2 cells. (A) BALB/c nude male mice were injected subcutaneously at the right back with HepG2 cells grown in T-CM or DMEM. After 9 days, tumor size was measured (n=3). (B) Tumors were isolated, chopped and seeded onto 100-mm cell culture plates 5 days after injection (n=3). Photographs were taken on a microscope 2 (upper) and 9 days (lower) after culture. Original magnification, x100. (C) Number of cell clusters on the cell culture plate was counted (n=3/mouse). (D) *In vitro* scratch wound healing assay was conducted. HepG2 cells were cultured in the presence or absence of T-CM and the migrated cells over the scratched area were observed after 24 and 48 h. Magnification, x40. (E) Wound closure area was calculated and compared. A total of >10 experiments were analyzed, and each experiment was repeated three times. Data were analyzed by paired t-test. *P<0.05 vs. control. (F) Wound width was measured and distance was calculated (n=10). Data are presented as the mean ± SEM and were analyzed by one-way ANOVA with multiple comparison by Sidak test. *P<0.05 and ***P<0.001. T-CM, tonsil-derived mesenchymal stem cell conditioned medium.

of miR-199a-3p, mir-214-3p, and miR-199-5p was higher in T-MSCs than in WJ-MSCs (Fig. 3A). The exosomes of T-MSCs had higher levels of hsa-miR-199a-3p than those of WJ-MSCs, as indicated by RT-qPCR and miRNA sequencing (Fig. 3B; Table I). To identify the effect of miR-199a-3p on HepG2 cell migration *in vitro*, transfected cells were treated with negative control or miR-199a-3p inhibitor. Treated cells were scratched and observed for 24 and 48 h following the addition of 10 μg/ml exosomes (Fig. 3C). The migrated distance in the control group (without exosomes) was greater and the wound area became smaller as time passed. By contrast, the wound area in the exosome-exposed group remained similar throughout the experiment. miR-199a-3p inhibitor reversed the effect of exosomes on migration (Fig. 3D). miR-199a-3p inhibitor reversed the effect of exosomes on migration after 48 h (Fig. 3E).

Exosomal microRNA hsa-miR-199a-3p suppresses expression of target genes in HepG2 cells. To investigate the molecular mechanism of how miR-199a-3p affects HepG2 cells, miR-199a-3p targets were predicted using the TargetScanHuman 7.2 database (targetscan.org/vert_72/). Hsa-miR-199a-3p was predicted to target Kelch-like family member 3, serpin family E member 2, pro-apoptotic WT1 regulator, vesicle-associated membrane protein 3, G protein subunit α12, BCAR3, CDK7, CD2-associated protein, CD151, FGF7, CXCL11, ITGB8, G3BP stress granule assembly factor 2, CDK17, mesenteric estrogen-dependent adipogenesis, collagen (COL) type IV α5 chain, RAB GTPase-activating protein 1, IL13RA1, ITGA3, SP1, TAO kinase 1, ITGA6, COL12A1 and histamine N-methyltransferase. The seed sequence of hsa-miR-199a-3p matched the sequence of the 3' untranslated regions of CD151, ITGA3 and ITGA6, suggesting that CD151, ITGA3 and ITGA6 were potential targets of miR-199a-3p (Fig. 4A). To confirm the effect of miR-199a-3p on T-MSCs, HepG2 cells were transfected with miR-199a-3p inhibitor or negative control inhibitor. Transfection efficiency of miR-199a-3p inhibitor was confirmed by the 87% decrease of the miR-199a-3p expression (Fig. S6). Expression of CD151, ITGA3 and ITGA6 in HepG2 cells was downregulated by EV treatment (Fig. 4B).

Discussion

Our previous studies reported several novel immune modulatory effects of T-MSCs and T-CM. For examples, tumor necrosis factor α inducible gene 6 protein expression in T-CM attenuates the acute graft-versus-host reaction (24);

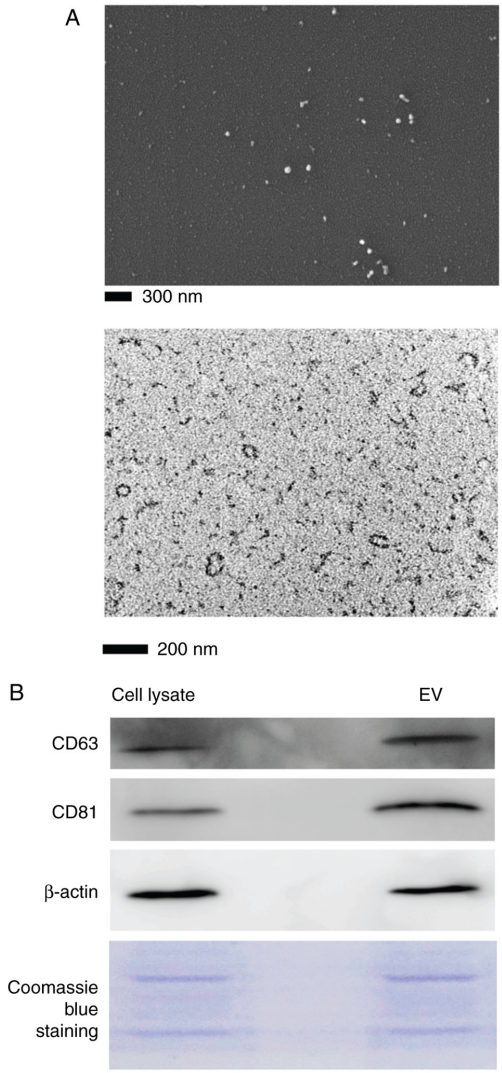

Figure 2. Characterization of T-MSC EVs. (A) Scanning (upper; magnification, x70,000) and transmission electron microscopy (lower; magnification, x200,000) images of EVs released from T-MSCs. (B) Immunoblot analysis of EV specific markers, CD63 (26 kDa) and CD81 (22-26 kDa), from cell lysates and EVs of T-MSCs. β-actin (42 kDa) and Coomassie blue staining gel were used as a loading control (5 μg/lane). T-MSC, tonsil-derived mesenchymal stem cell; EV, extracellular vesicle.

Table I. Top 30 miRs highly expressed in tonsil-derived mesenchymal stem cell extracellular vesicles.

Mature ID	Fold-change
hsa-miR-199a-3p	3609
hsa-miR-145-5p	3433
hsa-miR-24-3p	2612
hsa-miR-214-3p	2603
hsa-let-7b-3p	2448
hsa-miR-125a-5p	2196
hsa-miR-125b-5p	2068
hsa-miR-29b-3p	2020
hsa-miR-19b-3p	1902
hsa-miR-424-5p	1779
hsa-let-7a-3p	1648
hsa-miR-29a-3p	1575
hsa-miR-151a-3p	1517
hsa-let-7i-5p	1449
hsa-miR-126-5p	1390
hsa-miR-199a-5p	1220
hsa-miR-376c-3p	1213
hsa-miR-30a-3p	1060
hsa-miR-19a-3p	1039
hsa-miR-143-3p	915
hsa-let-7f-1-3p	913
hsa-miR-130a-3p	887
hsa-miR-30e-3p	794
hsa-miR-199b-5p	705
hsa-miR-409-3p	669
hsa-miR-92b-3p	618
hsa-miR-654-3p	607
hsa-miR-6126	603
hsa-miR-98-5p	584
hsa-miR-483-3p	567

miR, microRNA.

EBV-induced gene 3 stimulates regulatory B cells (25); and PD-L1 inhibits Th17-mediated autoimmune or skin inflammatory responses (6). Because all of these disease models for the immune regulatory effect of T-MSCs or T-CM are inflammatory conditions, the effect of T-CM on tumor growth was assessed in an animal model; T-MSCs inhibited tumor growth and HepG2 cell migration, potentially via miRNA containing EVs, in particular, miR-199a-3p.

EVs are nanometer-sized particles and mostly below the detection limit of conventional analysis methods, such as ultracentrifugation, filtration or precipitation. Therefore, to meet minimal experimental requirement, ISEV proposed MISEV guidelines for EV studies. EV are <100 or 200 nm (small EVs) or >200 nm (medium/large). EVs can be derived from tissue culture CM, biofluid or tissue. EV separation and concentration methods includes centrifugation, density gradient, chromatography, precipitation, filtration and antibody-based. For EV characterization, quantification (protein amount, particle number, lipid amount), global characterization (transmembrane or glycosylphosphatidylinositol-anchored protein or expected contaminants) and single EV characterization can be image-(electron microscopy) or non-image-based (nanoparticle tracking analysis, flow cytometry or Raman spectroscopy) (11). Functional studies can be quantitative comparison of activity of total fluid, EV-depleted fluid and EVs (11,26).

MSC regeneration is a secretome-based paracrine effect, and the use of MSC CM has become more common as a strategy to discover novel therapeutic targets. However, the heterogeneity of the MSC population promotes the use of its refined form, EVs, instead of CM or MSCs. Protein- and miRNA-enriched MSC-derived EV serve a role in maintaining homeostasis as stromal cells as well as in response to stimuli, such as injury or disease state. MSC-derived EVs serve a role in immune regulation, angiogenesis, proliferation and other processes (27). For immune regulation,

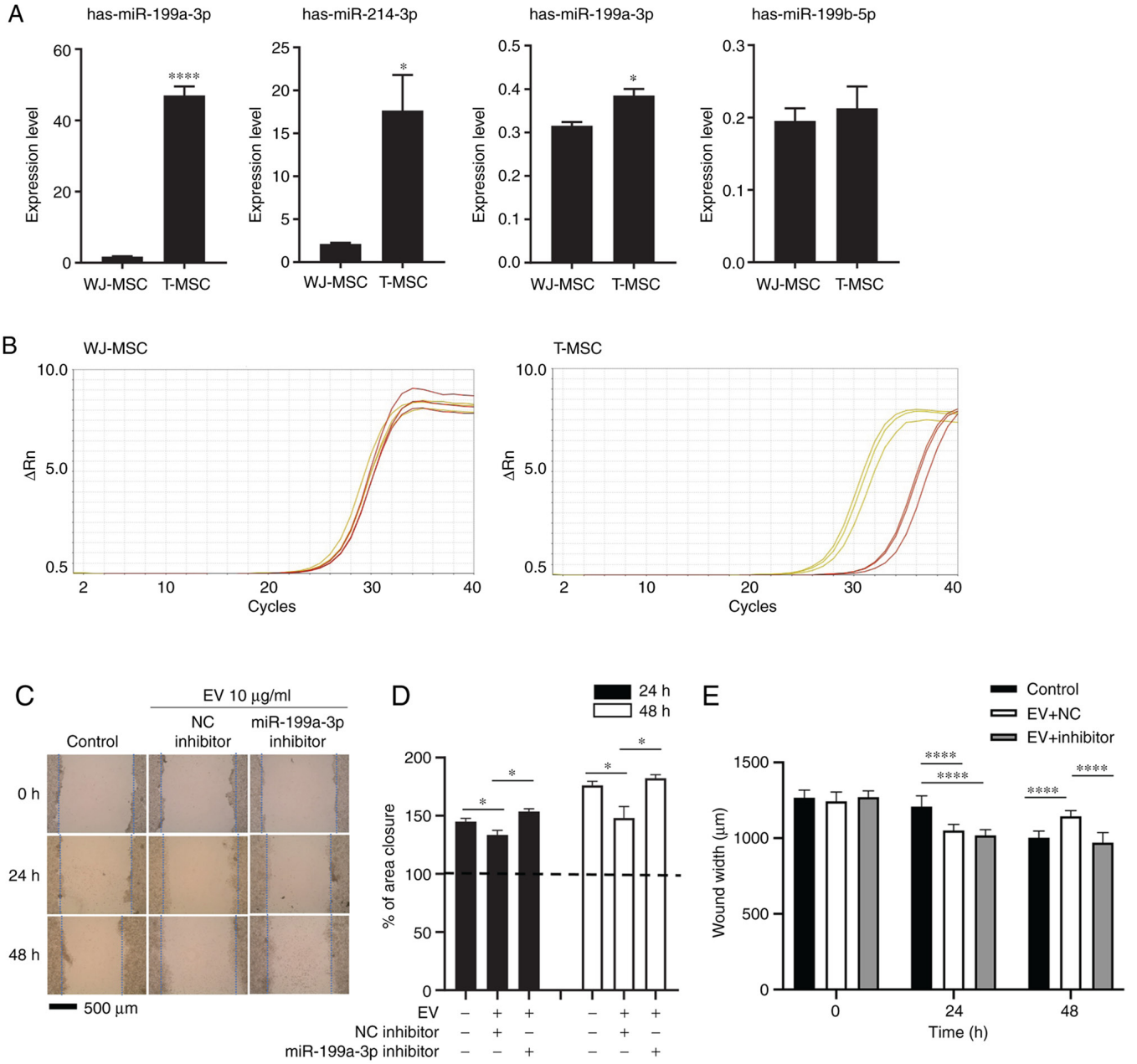

Figure 3. miR-199a-3p inhibitor attenuates the effect of T-MSC EVs on scratch wound healing assay. (A) EV RNA from WJ-MSCs and T-MSCs was extracted at 80% confluence and analyzed by reverse transcription-qquantitative PCR. Data are presented as the mean ± SEM and analyzed by Student t-test *P<0.05, ****P<0.0001. (B) Amplification plot. Yellow, hsa-miR-199a-3p; red, control (RNU6-1). (C) Migration of HepG2 cells following transfection and addition of EVs with NC or miR-199a-3p inhibitor. Magnification, x40. (D) Closure area was calculated after 24 or 48 h. A total of >10 fields of view were analyzed and each experiment was repeated three times. Statistical significance was determined by t test. (E) Wound width was measured and distance was calculated (n=10 per field). Data are presented as the mean ± SEM and analyzed by one-way ANOVA with multiple comparison by Sidak test *P<0.05, ****P<0.0001 vs. WJ-MSC. Untreated, miRNA NC- and miR-199a-3p inhibitor-treated HepG2 cells were used as the control, NC and inhibitor, respectively. miR, microRNA; T-MSC, tonsil-derived mesenchymal stem cell; EV, extracellular vesicle; WJ, Wharton's jelly; NC, negative control.

MSC-derived EVs deliver anti-inflammatory cytokine IL-10 and anti-inflammatory miRNAs (miRNA-21, miRNA-146a, miRNA-181c, miRNA-124a and miRNA-125b) (28). Pro-angiogenic miRNAs delivered by MSC-derived EVs include miRNA-126, miRNA-130a, miRNA-125a (inhibits angiogenic inhibitor Δ-like 4) and miRNA-31 [suppresses hypoxia-inducible factor (HIF)-1] (29). MSC-derived EVs also deliver mRNA from the PI3K/AKT/endothelial (eNOS pathway and trophic factors FGF1, VEGFA, VEGFR2, IL8, angiopoietin 1, E-selectin, CXCL16 and eNOS (30). MSC-derived EVs induce β-catenin activation but decrease MMP-9 mRNA in target cells (31). The targets of MSC-derived EV miRNAs are associated with cell death and growth and fibrosis via Wnt signaling, platelet-derived GF and TGF-β (32).

Previous reports indicated MSC-derived EVs both promote and inhibit tumor progression (33,34). The miRNAs or non-coding RNAs that are involved in cancer promotion include miR-1587 (glioma-associated MSCs), miRNA-21 and miRNA34a (blood and breast cancer MSCs), miR-221 (gastric cancer tissue-derived MSCs) and LINC00461 (multiple myeloma BM-MSCs) (35). Anti-tumor miRNAs

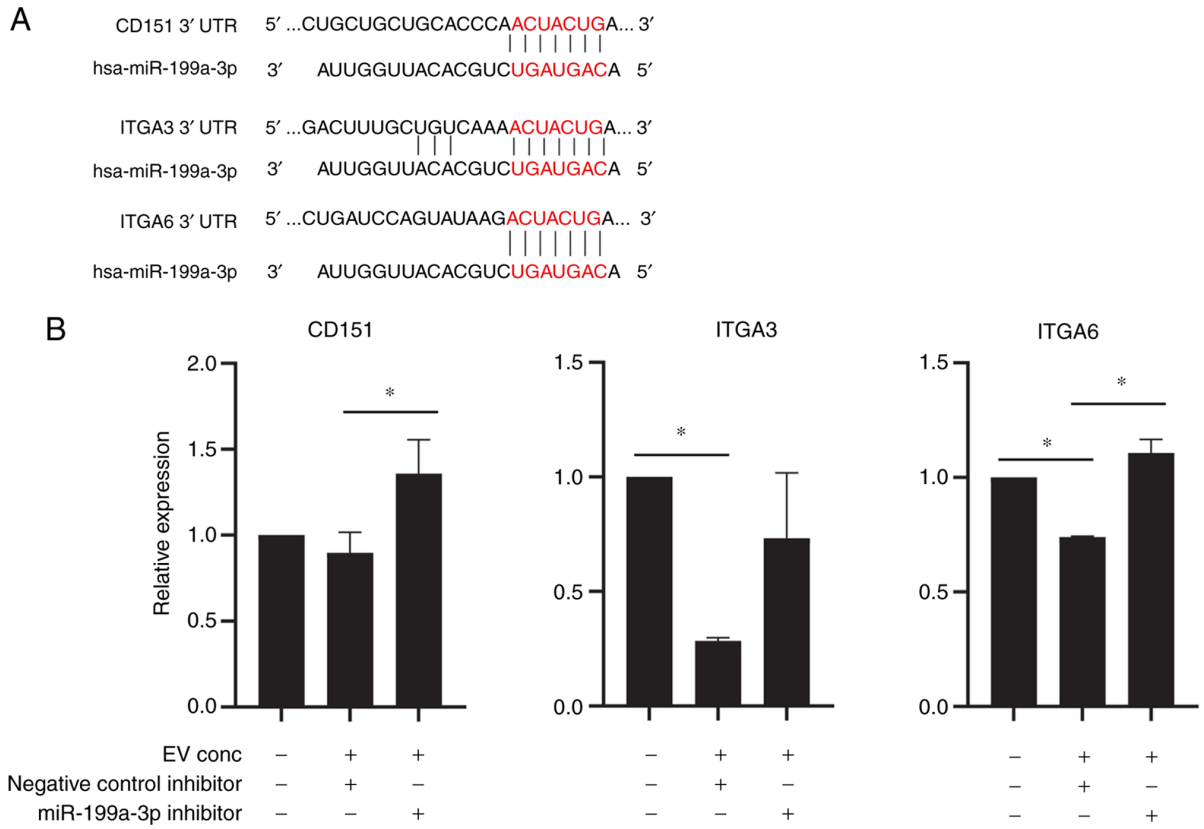

Figure 4. miR-199a-3p of tonsil-derived mesenchymal stem cell EVs suppresses target genes in HepG2 cells. (A) Sequence alignment of putative hsa-miR-199a-3p binding sites in the 3'UTR of CD151, ITGA3 and ITGA 6. (B) RNA was extracted and analyzed by reverse transcription-qquantitative PCR. Data are presented as the mean ± standard error of the mean. Statistical significance was determined by t test. *P<0.05. UTR, untranslated region; ITG, integrin; EV, extracellular vesicle.

from MSC-derived EVs include: miRNA-145 (from adipose tissue-derived MSCs in prostate cancer), miR-124 and miR-145 (from glioma cells), miR-100 (suppresses *in vitro* angiogenesis via mTOR/HIF-1α/VEGF in breast cancer), miR-23b and miR-222/223 (promote dormancy in breast cancer) (36,37). Therefore, T-MSC EVs may regulate cancer progression as indicated by highly enriched cancer pathway in KEGG analysis of miRNA target genes (Fig. S5).

miRNA-199a-3p was the most highly expressed miRNA in EVs isolated from T-MSCs and was more highly expressed in EVs from T-MSCs compared with those from WJ-MSCs. miRNA-199a-3p was also highly expressed in BM-MSC-derived EVs and has been found to inhibit cardiomyocyte apoptosis (32). Another report found the potential target of miR-199a-3p is ITGB8, which enhances cisplatin sensitivity in ovarian cancer (38). Because ITGs may affect cell growth and motility, CD151, ITGA3, and ITGA6 were selected from miRNA-199a-3p target genes for further investigation.

Tetraspanins do not have enzymatic activity or a canonical signaling pathway, but organize cytokine receptors, adhesion receptors and proteases (39). Tetraspanin CD151 is normally expressed in endothelial cells and platelets and overexpressed in cancer cells (40) and involved in membrane fusion, trafficking, cell motility and tumor development. CD151 interacts with MMP-14, cadherins, immunoglobulin proteins, other tetraspanins and ITGA3 and α6 (39). CD151-targeted monoclonal antibody 1A5 inhibits tumor cell motility and metastasis (41). CD151 association with ITGA6ß1 activates angiogenesis signaling (PI3K, Akt and NOS) and the invasion pathway (JNK, JUN and MMP-9). In addition, CD151 binds to α3ß1 and causes invasion and cytoskeletal reorganization (PKC, cell division cycle 42 and actin) (40). Although loss of CD151 decreases migration on laminin (42), ITG-free tetraspanin CD151 clustering is a strong regulator of motility in the absence of α3 expression but requires PKCα (43). Disruption of CD151-ITGA3 complex inhibits migration and invasion of lung adenocarcinoma cells *in vitro* via the FAK/p130Cas signaling pathway (44).

The present results suggested that miR-199a-3p-containing EVs from T-MSCs may exert a suppressive effect on HepG2 cell motility. Because EVs possess membrane structures that fuse cell membranes of target cells, EVs or modified EVs may enhance the therapeutic effect and cancer targeting (45) of isolated T-MSC-derived or miR-199a-3p-containing EVs, resulting in a tumor suppressive effect.

Acknowledgements

Not applicable.

Funding

The present study was supported by a grant from the Korea Health Technology R&D Project through the Korea Health

Industry Development Institute funded by the Ministry of Health & Welfare, Republic of Korea (grant no. HI18C2392); an intramural grant from the Ewha Education and Research Center for Infection (2019); and a National Research Foundation of Korea grant funded by the Korea Government (grant no. NRF-2021R1A2C1012551).

Availability of data and materials

The datasets used and/or analyzed during the current study are available from the corresponding author on reasonable request.

Authors' contributions

DWC and KAC performed experiments and wrote the manuscript. JK performed the experiments. HJL, YHK and JWP analyzed the data and wrote the manuscript. SYW designed the experiments and wrote the manuscript. KAC and SYW confirm the authenticity of all the raw data. All authors read and approved the final version of the manuscript.

Ethics approval and consent to participate

The experimental procedures were approved by the Animal Care and Use Committee of the College of Medicine, Ewha Womans University (approval no. EUM19-446) and by the Institutional Review Board of the Ewha University Medical Center (approval no. EUMC 2018-01-011-002).

Patent consent for publication

Not applicable.

Competing interests

The authors declare that they have no competing interests.

References

1. Caplan AI: Mesenchymal stem cells. J Orthop Res 9: 641-650, 1991.
2. Crisan M, Yap S, Casteilla L, Chen CW, Corselli M, Park TS, Andriolo G, Sun B, Zheng B, Zhang L, *et al*: A perivascular origin for mesenchymal stem cells in multiple human organs. Cell Stem Cell 3: 301-313, 2008.
3. Ryu KH, Cho KA, Park HS, Kim JY, Woo SY, Jo I, Choi YH, Park YM, Jung SC, Chung SM, *et al*: Tonsil-derived mesenchymal stromal cells: Evaluation of biologic, immunologic and genetic factors for successful banking. Cytotherapy 14: 1193-1202, 2012.
4. Oh SY, Choi YM, Kim HY, Park YS, Jung SC, Park JW, Woo SY, Ryu KH, Kim HS and Jo I: Application of tonsil-derived mesenchymal stem cells in tissue regeneration: Concise review. Stem Cells 37: 1252-1260, 2019.
5. Cho KA, Park M, Kim YH, Woo SY and Ryu KH: RNA sequencing reveals a transcriptomic portrait of human mesenchymal stem cells from bone marrow, adipose tissue, and palatine tonsils. Sci Rep 7: 17114, 2017.
6. Kim JY, Park M, Kim YH, Ryu KH, Lee KH, Cho KA and Woo SY: Tonsil-derived mesenchymal stem cells (T-MSCs) prevent Th17-mediated autoimmune response via regulation of the programmed death-1/programmed death ligand-1 (PD-1/PD-L1) pathway. J Tissue Eng Regen Med 12: e1022-e1033, 2018.
7. Caplan AI and Correa D: The MSC: An injury drugstore. Cell Stem Cell 9: 11-15, 2011.
8. Andrzejewska A, Lukomska B and Janowski M: Concise review: Mesenchymal stem cells: From roots to boost. Stem Cells 37: 855-864, 2019.
9. Gnecchi M, He H, Liang OD, Melo LG, Morello F, Mu H, Noiseux N, Zhang L, Pratt RE, Ingwall JS and Dzau VJ: Paracrine action accounts for marked protection of ischemic heart by Akt-modified mesenchymal stem cells. Nat Med 11: 367-368, 2005.
10. Goolaerts A, Pellan-Randrianarison N, Larghero J, Vanneaux V, Uzunhan Y, Gille T, Dard N, Planès C, Matthay MA and Clerici C: Conditioned media from mesenchymal stromal cells restore sodium transport and preserve epithelial permeability in an in vitro model of acute alveolar injury. Am J Physiol Lung Cell Mol Physiol 306: L975-L985, 2014.
11. Théry C, Witwer KW, Aikawa E, Alcaraz MJ, Anderson JD, Andriantsitohaina R, Antoniou A, Arab T, Archer F, Atkin-Smith GK, *et al*: Minimal information for studies of extracellular vesicles 2018 (MISEV2018): A position statement of the international society for extracellular vesicles and update of the MISEV2014 guidelines. J Extracell Vesicles 7: 1535750, 2018.
12. Nakamura Y, Miyaki S, Ishitobi H, Matsuyama S, Nakasa T, Kamei N, Akimoto T, Higashi Y and Ochi M: Mesenchymal-stem-cell-derived exosomes accelerate skeletal muscle regeneration. FEBS Lett 589: 1257-1265, 2015.
13. Asgarpour K, Shojaei Z, Amiri F, Ai J, Mahjoubin-Tehran M, Ghasemi F, ArefNezhad R, Hamblin MR and Mirzaei H: Exosomal microRNAs derived from mesenchymal stem cells: Cell-to-cell messages. Cell Commun Signal 18: 149, 2020.
14. Mathivanan S, Fahner CJ, Reid GE and Simpson RJ: ExoCarta 2012: Database of exosomal proteins, RNA and lipids. Nucleic Acids Res 40 (Database Issue): D1241-D1244, 2012.
15. Whiteside TL: The tumor microenvironment and its role in promoting tumor growth. Oncogene 27: 5904-5912, 2008.
16. Balkwill FR, Capasso M and Hagemann T: The tumor microenvironment at a glance. J Cell Sci 125: 5591-5596, 2012.
17. Keshtkar S, Azarpira N and Ghahremani MH: Mesenchymal stem cell-derived extracellular vesicles: Novel frontiers in regenerative medicine. Stem Cell Res Ther 9: 63, 2018.
18. Bruno S, Collino F, Deregibus MC, Grange C, Tetta C and Camussi G: Microvesicles derived from human bone marrow mesenchymal stem cells inhibit tumor growth. Stem Cells Dev 22: 758-771, 2013.
19. Alzahrani FA, El-Magd MA, Abdelfattah-Hassan A, Saleh AA, Saadeldin IM, El-Shetry ES, Badawy AA and Alkarim S: Potential effect of exosomes derived from cancer stem cells and MSCs on progression of DEN-induced HCC in rats. Stem Cells Int 2018: 8058979, 2018.
20. Kim YH, Cho KA, Lee HJ, Park M, Shin SJ, Park JW, Woo SY and Ryu KH: Conditioned medium from human tonsil-derived mesenchymal stem cells enhances bone marrow engraftment via endothelial cell restoration by pleiotrophin. Cells 9: 221, 2020.
21. He XX, Chang Y, Meng FY, Wang MY, Xie QH, Tang F, Li PY, Song YH and Lin JS: MicroRNA-375 targets AEG-1 in hepatocellular carcinoma and suppresses liver cancer cell growth in vitro and in vivo. Oncogene 31: 3357-3369, 2012.
22. Ramsköld D, Luo S, Wang YC, Li R, Deng Q, Faridani OR, Daniels GA, Khrebtukova I, Loring JF, Laurent LC, *et al*: Full-length mRNA-Seq from single-cell levels of RNA and individual circulating tumor cells. Nat Biotechnol 30: 777-782, 2012.
23. Livak KJ and Schmittgen TD: Analysis of relative gene expression data using real-time quantitative PCR and the 2(-Delta Delta C(T)) method. Methods 25: 402-408, 2001.
24. Cho KA, Kim YH, Park M, Kim HJ, Woo SY, Park JW and Ryu KH: Conditioned medium from human palatine tonsil mesenchymal stem cells attenuates acute graft-vs-host disease in mice. Mol Med Rep 19: 609-616, 2019.
25. Cho KA, Lee JK, Kim YH, Park M, Woo SY and Ryu KH: Mesenchymal stem cells ameliorate B-cell-mediated immune responses and increase IL-10-expressing regulatory B cells in an EBI3-dependent manner. Cell Mol Immunol 14: 895-908, 2017.
26. Poupardin R, Wolf M and Strunk D: Adherence to minimal experimental requirements for defining extracellular vesicles and their functions. Adv Drug Deliv Rev 176: 113872, 2021.
27. Ferreira JR, Teixeira GQ, Santos SG, Barbosa MA, Almeida-Porada G and Gonçalves RM: Mesenchymal stromal cell secretome: Influencing therapeutic potential by cellular pre-conditioning. Front Immunol 9: 2837, 2018.
28. Tahamtan A, Teymoori-Rad M, Nakstad B and Salimi V: Anti-inflammatory MicroRNAs and their potential for inflammatory diseases treatment. Front Immunol 9: 1377, 2018.
29. Suárez Y and Sessa WC: MicroRNAs as novel regulators of angiogenesis. Circ Res 104: 442-454, 2009.

30. Gu H, Ji R, Zhang X, Wang M, Zhu W, Qian H, Chen Y, Jiang P and Xu W: Exosomes derived from human mesenchymal stem cells promote gastric cancer cell growth and migration via the activation of the Akt pathway. Mol Med Rep 14: 3452-3458, 2016.
31. Wu P, Zhang B, Shi H, Qian H and Xu W: MSC-exosome: A novel cell-free therapy for cutaneous regeneration. Cytotherapy 20: 291-301, 2018.
32. Ferguson SW, Wang J, Lee CJ, Liu M, Neelamegham S, Canty JM and Nguyen J: The microRNA regulatory landscape of MSC-derived exosomes: A systems view. Sci Rep 8: 1419, 2018.
33. Zhao R, Chen X, Song H, Bie Q and Zhang B: Dual role of MSC-derived exosomes in tumor development. Stem Cells Int 2020: 8844730, 2020.
34. Christodoulou I, Goulielmaki M, Devetzi M, Panagiotidis M, Koliakos G and Zoumpourlis V: Mesenchymal stem cells in preclinical cancer cytotherapy: A systematic review. Stem Cell Res Ther 9: 336, 2018.
35. Vallabhaneni KC, Penfornis P, Dhule S, Guillonneau F, Adams KV, Mo YY, Xu R, Liu Y, Watabe K, Vemuri MC and Pochampally R: Extracellular vesicles from bone marrow mesenchymal stem/stromal cells transport tumor regulatory microRNA, proteins, and metabolites. Oncotarget 6: 4953-4967, 2015.
36. Takahara K, Ii M, Inamoto T, Nakagawa T, Ibuki N, Yoshikawa Y, Tsujino T, Uchimoto T, Saito K, Takai T, *et al*: microRNA-145 mediates the inhibitory effect of adipose tissue-derived stromal cells on prostate cancer. Stem Cells Dev 25: 1290-1298, 2016.
37. Cai QQ, Dong YW, Wang R, Qi B, Guo JX, Pan J, Liu YY, Zhang CY and Wu XZ: MiR-124 inhibits the migration and invasion of human hepatocellular carcinoma cells by suppressing integrin αV expression. Sci Rep 7: 40733, 2017.
38. Cui Y, Wu F, Tian D, Wang T, Lu T, Huang X, Zhang P and Qin L: miR-199a-3p enhances cisplatin sensitivity of ovarian cancer cells by targeting ITGB8. Oncol Rep 39: 1649-1657, 2018.
39. Hemler ME: Tetraspanin functions and associated microdomains. Nat Rev Mol Cell Biol 6: 801-811, 2005.
40. Kumari S, Devi G V, Badana A, Dasari VR and Malla RR: CD151-A striking marker for cancer therapy. Biomark Cancer 7: 7-11, 2015.
41. Zijlstra A, Lewis J, Degryse B, Stuhlmann H and Quigley JP: The inhibition of tumor cell intravasation and subsequent metastasis via regulation of in vivo tumor cell motility by the tetraspanin CD151. Cancer Cell 13: 221-234, 2008.
42. Winterwood NE, Varzavand A, Meland MN, Ashman LK and Stipp CS: A critical role for tetraspanin CD151 in alpha3beta1 and alpha6beta4 integrin-dependent tumor cell functions on laminin-5. Mol Biol Cell 17: 2707-2721, 2006.
43. Zevian SC, Johnson JL, Winterwood NE, Walters KS, Herndon ME, Henry MD and Stipp CS: CD151 promotes α3β1 integrin-dependent organization of carcinoma cell junctions and restrains collective cell invasion. Cancer Biol Ther 16: 1626-1640, 2015.
44. Peng D, Li PC, Liu T, Zeng HS, Fei YJ, Liu ZX and Zuo HJ: Key role of CD151-integrin complex in lung cancer metastasis and mechanisms involved. Curr Med Sci 40: 1148-1155, 2020.
45. You B, Xu W and Zhang B: Engineering exosomes: A new direction for anticancer treatment. Am J Cancer Res 8: 1332-1342, 2018.